RSC Advances

This is an *Accepted Manuscript*, which has been through the Royal Society of Chemistry peer review process and has been accepted for publication.

Accepted Manuscripts are published online shortly after acceptance, before technical editing, formatting and proof reading. Using this free service, authors can make their results available to the community, in citable form, before we publish the edited article. This *Accepted Manuscript* will be replaced by the edited, formatted and paginated article as soon as this is available.

You can find more information about *Accepted Manuscripts* in the Information for Authors.

Please note that technical editing may introduce minor changes to the text and/or graphics, which may alter content. The journal's standard Terms & Conditions and the Ethical guidelines still apply. In no event shall the Royal Society of Chemistry be held responsible for any errors or omissions in this *Accepted Manuscript* or any consequences arising from the use of any information it contains.

ROYAL SOCIETY OF CHEMISTRY

www.rsc.org/advances

Improvement of the thermoelectric performance of InSe-based alloys doped with Sn

Xiaojing Hou[1,2], Shaoping Chen[1*], Zhengliang Du[2], Xianglian Liu[2], Jiaolin Cui[2*]

Received (in XXX, XXX) Xth XXXXXXXXX 200X, Accepted Xth XXXXXXXXX 200X
DOI: 10.1039/b000000x

ABSTRACT Here we present InSe-based alloys $InSeSn_x$ (x=0~0.02) with improved thermoelectric performance upon Sn's preferential occupation on In lattice sites. This improvement is attributed to the enhancement in carrier concentration (n) and reduction in lattice thermal conductivity (κ_L). However, the enhancement in n is limited due to the presence of the intermediate band in the middle of the bandgap, which acts as an annihilation center for electrons and holes. The reduction in κ_L is caused by increased phonon scattering on the newly-created defect Sn_{In}^+. As a result, we attain the highest ZT value of 0.23 at x=0.01 @ 830K, which is about 2.9 times that of virgin InSe.

1. Introduction

Thermoelectric (TE) materials can directly convert heat to electricity and vice versa, therefore they have attracted much attention in energy harvesting. However, the conversion efficiency of TE semiconductors, which are characterized by the dimensionless figure of merit (ZT), ZT= $T\alpha^2\sigma/\kappa$, where α is the Seebeck coefficient, σ the electrical conductivity, κ the total thermal conductivity consisting of lattice (κ_L) and electronic part (κ_e), and T the absolute temperature, is rather low compared to those of traditional heat engines. To significantly improve the ZT value is challenging because the Seebeck coefficient (α) and electrical conductivity (σ), which vary inversely with carrier concentration (n), are interdependent.

Although many approaches to enhancing ZT have been developed, including the enhancement of Seebeck coefficients (by modifying the band structure,[1] band convergence,[2] quantum confinement effects[3] and electron energy barrier filtering[4]), and reduction of lattice thermal conductivity (by nanostructuring[5] and all-scale hierarchical architecturing[6]), there still remains necessity to explore new materials, especially wide gap semiconductors, which are potentially competent TE candidates.

In recent years indium selenides have been paid increasing attention due to their intrinsic structural characteristics, including phases, crystal structures and structural imperfection.[7] Among them In_4Se_3- (ZT=1.48 @ 705K,[8(a)] and 1.11 @ 723K[8(b)]) and In_2Se_3-based (ZT=1.23 @ 916K)[9] alloys have already presented their potential TE performance. InSe, which is one of indium selenides, crystallizes in a layered structure where each layer contains sublayers closely packed with two In and two Se, in a stacking sequence Se–In–In–Se, whereas the bonding between two adjacent layers is of the weak Van der Waals type. Therefore, the materials of InSe family usually present anisotropic characteristics. Although there are some defects acting as donors in not purposely-doped InSe, such as interstitial In atom (In_i)[10] and Se vacancy (V_{se})[11], the virgin n-type InSe crystal gives much lower carrier concentration (n) at room temperature (RT) (10^{14}~10^{15}cm^{-3})[10,12] than good TE candidates do, which usually have n values as high as 10^{19}~10^{20}cm^{-3}.[13] Hence it is strongly necessary to enhance the carrier concentration in order to improve the TE performance of InSe based alloys.

Some investigations [10,11] suggest that element Sn is the most suitable donor impurity in InSe as it permits to reduce the resistivity of the material without strongly affecting the electron mobility (μ) through forming shallow donor levels, and some indicate that only a small part of Sn gets into the lattice while the rest remains as interlayer precipitate planes forming large planar defects.[11] However, Gridin *etc.*[14] propose that there might exist some deep impurity levels in InSe upon Sn(Zn)-doping. Such deep impurity levels could provide annihilation centres for electrons and holes, and thereby reduce the carrier concentration. Besides, the impurities from the same column (such as Sn and Pb) in InSe act quite differently, the first as a donor and the second as an acceptor.[11] Therefore, the action of Sn in InSe is still unclear and needs to be probed. In order to improve the TE performance of InSe-based materials, we should figure out the conducting mechanism of both carrier and phonons when impurity, such as Sn, acts.

T In this work, we have measured carrier concentrations and calculated band structures upon proper incorporations of Sn into different lattice sites in InSe, through which we have been able to determine the preferential occupation of Sn in the InSe lattice. The incorporation of Sn, which creates an active donor defect Sn_{In}^+, increases carrier concentration (n) and phonon scattering, and thereby improves TE performance drastically.

2. Experimental

2.1 Sample preparations

The compounds $InSeSn_x$ (x=0, 0.005, 0.01, 0.02), which consist of three elements In, Sn and Se with a purity of 99.999%, were synthesized in different vacuum silica tubes at 1273K for 24h, during which time a 30s rocking time was conducted every 1 h to ensure homogenous composition. The melt was then quenched down from 1273K to 853K to prevent peritectic reaction at 873K from forming In_6Se_7.[12(a)] Subsequently, the melt was held at 853K for another 24h to form single phase InSe, and finally it was cooled down at a rate of 20K/h to room temperature (RT). The as-solidified ingots were pulverized and then ball milled in stainless steel bowls that contain petroleum ether at a rotation rate

RSC Advances Accepted Manuscript

of 350 rpm for 5h. The dried powders were sintered by using spark plasma sintering apparatus (SPS-1030) under a pressure of 60 MPa and at the highest temperature of 853 K. The densities (d) of the sintered samples, which were measured using Archimedes' method, are more than 95% of theoretical one. Two sintered blocks with sizes of ϕ~13.0 mm × ~14.0 mm and ϕ20 mm × 3.0 mm were cut into 3 mm-wide slices measuring 2.5 mm×12 mm for electrical property measurements (along ($C_{//}$) and perpendicular to the pressing direction ($C\perp$)), and those with ϕ~10.0 mm × 2.0 mm in both $C_{//}$ and $C\perp$ were obtained for thermal diffusivity measurements.

2.2 Compositional and Structural analyses

The structural analysis of the powders was made using a powder X-ray diffractometer (D8 Advance) along with small angle X-ray diffractions operating at 50 kV and 40 mA. Cu Ka radiation (l = 0.15406 nm) and a scan rate of 4° min^{-1} were used to record the patterns ranging from 10° to 140°. The chemical compositions were determined using an electron probe micro-analyzer (EPMA) (S-4800, Hitachi, Japan) with an accuracy of ~97%. X-ray photoelectron spectroscopy (XPS) measurements were performed on an AXIS ULTRA DLD equipped with a monochromatic Al Ka X-ray source (30 mA, 15 kV) and a hybrid lens. Samples were sputter-cleaned with an Ar+ ion beam until the core-line peaks associated with surface oxides were no longer observed in the XPS spectra. High-resolution core-line spectra of In3$d_{5/2}$, Sn3$d_{5/2}$, and Se3d were collected. In this work, four samples (x=0, 0.005, 0.01, 0.02) were examined, and pure InSe (x=0) was examined for comparison.

The absorption coefficient measurements were carried out using a Perkin-Elmer Lambda 950 UV-VIS-NIR spectrophotometer, and absorption spectra for the powders were recorded between the visible and infrared regions (200–1500 nm).[15]

When calculating the band structures, PW91/ GGA functional, implemented in the VASP software package, was used, and the $5s^2 5p^2$, $5s^2 5p^1$ and $4s^2 4p^4$ were each treated as valence states of Sn, In and Se. The plane-wave basis set cutoff is 450 eV and a k mesh of 7 × 7 × 2. The Monkhost− Pack mesh 49 sampling with 1 × 1 × 21 k-points in a string Brillouin zone (x, y, z directions, respectively) is employed. Basically, there are three arrangements of Sn occupation, which are on the interstitial In (In_i), In (Sn_{In}) and Se (Sn_{Se}) lattice sites, each corresponding to the chemical formulas of $In_{16}Se_{16}Sn$, $In_{15}Se_{16}Sn$ and $In_{16}Se_{15}Sn$ (equivalent to the Sn content x=~0.033).

2.3 TE transport property measurements

The Seebeck coefficients (α) and electrical conductivities (σ) as a function of temperature were measured using an ULVAC ZEM-3 instrument system in a helium atmosphere between RT and ~830K. A temperature difference of approximately 5°C was applied between the two terminals of the samples in order to measure the Seebeck coefficient, whereas the electrical conductivity was measured using the four-probe method. The measurement uncertainties are: 5% for α and 6% for σ. The total thermal conductivities (κ) at RT~832K, which were calculated as the product of the material densities, specific heats and thermal diffusivities (with uncertainty below ~12%), were measured using a TC-1200RH. The total uncertainty for ZT is ~16%. The lattice contributions (κ_L) were obtained by subtracting the electronic part (κ_e) from the total κ, i.e., $\kappa_L = \kappa_L$-κ_e. Here κ_e is expressed by the Wiedemann–Franz law, $\kappa_e = L_0 \sigma T$, where L_0 is the Lorenz number, which was estimated to be 1.5×10^{-8} WΩK^{-2} when taking the fact into account that the virgin InSe with a simple parabolic band model is close to nondegenerate limit.[9,16].

The parameters were finalized after several repeated measurements using different samples.

The Hall coefficient (R_h) measurements at RT, were performed on rectangular samples in size of 2 × 2 × 7 mm^3, were conducted on a Physical Property Measurement System (PPMS, Model-9) using a four probe configuration with a magnetic field sweeping between ±2.0T. The Hall mobility (μ) and carrier concentrations (n) were subsequently calculated based on the relations $\mu = |R_h|\sigma$ and $n = 1/(R_h e)$ respectively, where e is the electron charge. The current and Hall voltage leads were fine copper wires, and the contacts were made of silver paste.

3. Results and discussions

3.1 Compositional and structural analyses

The mapping pictures and EDAX spectrum for $InSeSn_x$ (x=0, 0.01) are demonstrated in Fig.S1(a-d). The chemical compositions at x=0 and 0.01 taken from mappings of EPMA are shown in Table.S1. The analysis reveals that there is a little deficiency in Se and an excess in In. Generally, the relative molars of In, Sn and Se identified are close to nominal ones, which suggests that the compositions at the final samples are almost as intended. XRD analysis shows that materials exhibit hexagonal InSe-based solid solution (space group: $P6_3$ /mmc, PDF:34-1431) in all the composition range (x=0~0.02), as shown in Fig.1a. With the Sn content increasing, both the lattice constant a (~3.996Å) and volume of unit cell (V=~230.0Å) remain almost unchanged, while c tends to decrease from 16.626 to 16.614Å (see Fig.1b). The values of a and c is in good agreement with those reported in *ref*.(17). The samll change in c implies that the element Sn has been incorporated into In or Se lattice sites, rather than into the weak Van der Waals space. Furthermore, we have not identified any detectable peak shifts below 2θ=9° (the results are not shown here) with small angle X-ray diffraction analyses.

The absorption coefficient spectra $A(hv)$ are shown in Fig.2(a), where A is the absorption coefficient and hv photon energy. In the spectra $A(hv)$ we have observed two absorption thresholds (One is around 1.24eV and the other on high energy side 1.50eV), instead of three edges observed by Balkanski.[18] The presence of two edges, which is likely originated from the 3d orbital splitting of the Se atoms,[19] results in two sets of bandgap values (E_g). The $E_g^{'}$ value, which fits the first edge (~1.50eV), reduces slightly from 1.01eV to 0.95eV (Fig.2(b)); while the second $E_g^{''}$ value, which fits the second one (~1.24eV), tends to reduce from 1.10eV to 1.03eV as x value increases (Fig.2(c)). Although both the bandgaps bears limited relevance to the composition, the measured E_g value of pure InSe (1.01~1.10eV) is about ~0.30eV lower than those reported (~1.35eV[18(a)] and ~1.20eV for Sn-containing InSe,[18(b)] where the Fermi level is assumed to lie in the top of the valence band maximum).

In order to have a thorough understanding of the incorporation of Sn in InSe lattice, we have analyzed the oxidation states of In, Sn and Se using In3$d/_{5/2}$, Sn3$d/_{5/2}$ and Se3d XPS spectra in $InSeSn_x$ (x=0, 0.005, 0.01, 0.02), as shown in Fig.S2. The average binding energy (BE) values with uncertainties estimated at ~±0.01 eV are listed in Table S2, in which we have observed that the BE values of In3d (444.44~444.73eV) (Fig.S2(a)) are roughly equal to those of In^{3+} in $CuInSe_2$ (444.70eV)[20] and 444.9eV in $In(OH)_3$.[21] Therefore, the obtained spectra can be assigned to In^{3+} cation. Each of the Se 3d spectra is clearly split into a resolved doublet (3$d_{5/2}$ and 3$d_{3/2}$ levels), with the BE values of Se3$d_{5/2}$ around 53.85eV and those of Se3$d_{3/2}$ 54.52eV, as shown in Fig.S2(b). These values are in good agreement with those of anionic Se in $Zn_{1-x}Mn_xCr_2Se_4$[22] and Se^{2-} (GeSe: ~54.5eV; Bi_2Se_3: ~54.2eV),[23] which confirms the existence of anionic Se^{2-}. Besides, there are no visible shifts of the doublet peak as Sn content increases. The BE values of Sn3d, which are determined

This journal is © The Royal Society of Chemistry [year]

RSC Advances Accepted Manuscript

by XPS peaks, are roughly equal to 486.0~487.0eV, close to that of Sn^{4+} (SnO_2: 486.0~486.3eV),[24] though these peaks are unconspicuous and a little difficult to identify due to limited Sn content in InSe, shown in Fig.S2(c).

When Sn^{4+} exists in the InSe crystal, there are basically three ways of arrangements in InSe lattice sites, that is, on the interstitial In (In_i), In and Se lattice sites. To determine the exact occupation site of Sn in InSe lattices, we have calculated the band structures upon Sn occupations in different sites. The results are shown in Fig.3. The band structure of virgin InSe is calculated for comparison (Fig.3a), in which case a direct band gap is observed with E_g= ~0.51eV and the Fermi level (*F*r) is just located at the top of the valence band maximum (VBM). When Sn occupies interstitial In sites, the bandgap narrows by lifting both the *F*r and VBM, and lets E_g= ~0 eV, (see Fig.3(b)), which indicates semimetal behaviour of the material. When Sn presumably occupies In lattice sites, the *F*r is lifted to the conduction band with the bandgap E_g= ~0.88eV(Fig.3c). Besides, there appears an intermediate band in the middle of the bandgap, which is approximately 0.34eV above the valence band edge. This deep level can be due to an isolated substitutional donor, which undergoes a shallow-to-deep transition under certain conditions of hydrostatic pressure.[25] The formation of the intermediate band might result from the creation of the In-Sn pockets via the incorporation of Sn in crystal lattice.[14(a)] However, this impurity level could act as an annihilation centre for electrons and holes and it does no help to the carrier concentration enhancement. Fig.3(d) presents the band structure with Sn occupying Se lattice sites, where we have observed the lowering of the *F*r towards the valence band, indicating p-type conducting behaviour. However, the VBM approaches to conducting band minimum (CBM), which leads to E_g= ~0 eV.

3.2 TE Transport properties

In the present work we failed to measure the *n* values at RT because the electrical conductivities of $InSeSn_x$ in question are too low. Therefore, we have measured the carrier concentrations (*n*) and mobility (μ) at 360K, the results of which are shown in Table 1, where we observe that with Sn content increasing from *x*=0 to *x*=0.005 the carrier concentration (*n*) increases from 2.57×10^{20} (m^{-3}) to 9.14×10^{20}(m^{-3}) in $C_\perp$ and from 1.15×10^{20} (m^{-3}) to 7.23×10^{20} (m^{-3}) in $C_{//}$ respectively, after which the *n* value tends to decrease with *x* value increasing. Likewise, the mobility (μ), which varies in the same way as carrier concentration, reaches the highest at *x*=0.005. Besides, both the carrier concentration (*n*) and mobility (μ) are about 1~2 orders of magnitude lower than those reported at RT[10,11].

Fig.4 is the plot of TE performance ($C_\perp$) perpendicular to the pressing direction, where we observe that the absolute Seebeck coefficients ($|\alpha|$), all of which decrease with the measuring temperature, bear little relevance to the chemical composition above 550K. At ~815K the α value is ~ -440.0(μV/K), as shown in Fig.4(a). The electrical conductivity (σ) increases slightly from 420.0 ($\Omega^{-1}m^{-1}$) at *x*=0 to 511.0 ($\Omega^{-1}m^{-1}$) at *x*=0.005 at 815K, as shown in Fig.4(b). Although the incorporation of Sn has a limited influence on the electrical property, it exerts a profound impact on the lattice thermal conductivity (κ_L), as shown in Fig.4(c). First, we have observed the bipolar effect at high temperatures, as the κ_L value for the virgin InSe shows an increasing tendency with the increase of temperature above 600K. Second, the κ_L value reduces drastically from 1.09 $Wk^{-1}m^{-1}$ at *x*=0 to ~0.44$Wk^{-1}m^{-1}$ at *x*=0.005~0.01@ ~815K. However, the κ_L value of the sample at *x*=0.02, which is much higher, decreases from 4.72 $Wk^{-1}m^{-1}$ at RT to 2.38$Wk^{-1}m^{-1}$ at ~815K. In addition, the lattice contributions takes more than ~90% in total thermal conductivities, as shown in Fig.4c and Fig.S3.

Combining the three physical parameters (α,σ and κ) we attain the dimensionless figure of merits (ZT), which is shown in Fig.4(d). The sample at *x*=0.005 gives the highest ZT value (~0.20) at 815K, while the virgin InSe gives only 0.06. The highest ZT value for InSe based alloys is much lower than those of other In-Se based families, such as Zn-doped α-In_2Se_3 (ZT=1.23 @ 916K)[9] and In_4Se_3-based alloys (1.48 @ 705K[8(a)], 1.40 @ 733K[26(a)], 1.53 @ 698K[26(b)]), and also lower than that for one of the $In_{1.3-x}Sn_xSe$ alloys (*x*=0.05) (ZT=0.66 @ 700K).[27] However, these materials are actually more In_4Se_3- than InSe-based alloys, since the chemical compositions of $In_{1.3}Se$ is closer to In_4Se_3 than to InSe, even though InSe and In_4Se_3 bear similar structures.

Similarly, the temperature dependences of the Seebeck coefficients (α) in $C_{//}$ are almost identical to those in $C_\perp$ (Fig.5(a)), and the electrical conductivities (σ) are only about 120.0($\Omega^{-1}m^{-1}$) lower for the corresponding Sn content (Fig.5(b)) at 830K. Furthermore, above 620K the samples at *x*=0.005 and 0.01 give lower lattice contributions κ_L than Sn-free InSe, whereas the sample at *x*=0.02 gives much higher κ_L values at high temperatures, and at ~830K it gives 1.55$Wk^{-1}m^{-1}$, which is about three times that of Sn-free InSe (Fig.5(c)). Likewise, the lattice contributions (κ_L) in $C_{//}$ play a dominant role in carrying heat, as shown in (Fig.S4). The highest ZT value in $C_{//}$ is 0.23 at *x*=0.01 @ ~830K (Fig.5(d)), a little higher than that in $C_\perp$.

The improvement in TE performance is closely related to the Sn incorporation in InSe. When Sn is assumed to occupy In lattice sites, we have observed a lift of *F*r to the conduction band (Fig.3(c)) through the band structure calculation, which indicates that the electrons can occupy those extended states that give rise to the degenerate behaviour of the electron concentration. However, the measurement reveals that the unexpected enhancement in the carrier concentration does not agree to our assumption (Table 1) because the highest *n* value is still in the order of magnitude ~$10^{21}m^{-3}$. Despite that the estimated bandgaps, which are usually lower than those from measurements because of Local Density Approximation (LDA)/GGA problem, all tend to narrow no matter where Sn occupies In or Se lattice sites. Nevertheless, the E_g values will vary widely depending on the occupation site of Sn (see Fig.3). If we compare the E_g values from calculations with those from measurements, and also take the measured *n* values into account, we believe that Sn prefers the In to Se lattice sites. It is not only because the bandgap (0.88eV) through calculation is closer to the measured one (0.95~1.03eV), but we have also observed the formation of an intermediate band acting as annihilation centres for electrons and holes, which is exactly what leads to a limited enhancement in *n*. Moreover, Sn is least likely to occupy the interstitial In sites (In_i), because such an incorporation tends to yield semimetal behaviour of the materials.

The preferential occupation of Sn on the In sites is in agreement with the proposed configuration by Segura[11], who suggested that in the Sn-doped InSe the suitable configuration is one couple of Sn atoms substitute a couple of neighbour In atoms. Based on this configuration, an active donor defect Sn_{In}^+ forms and thereby distorts the lattice structure.

Although the lattice distortion increases carrier scattering factor (γ) and thereby exerts a positive effect on the Seebeck coefficients, such an effect is neutralized by a negative one caused by the enhancement in carrier concentration (*n*), which is why we have observed a subtle change in the α value over the measuring temperature range. On the other hand, the enhancement in carrier concentration (*n*) is limited because of the formation of the intermediate band. Therefore, we have only

RSC Advances Accepted Manuscript

observed a subtle/minimal improvement in electrical conductivity. Besides, both the n and μ values reach the highest at the same Sn content (x=0.005), which might be due to the fact that Sn occupation in the In sites facilitates the cationic interdiffusion, which promotes the transport of carriers.[28] However, this argument needs clarification after further investigations. Also, the newly-created defect Sn_{In}^{+} acts not only as scattering centers for carriers, but also as scattering centers for phonons, which thereby reduces the lattice contribution κ_L when Sn content increases to x=0.005~0.01. However, in the highly Sn-doped InSe the electron concentration could reach a saturation at a certain value.[10(a)] This implies that there might exist other substitutional configurations of Sn in InSe which help form acceptor centers in the highly-doped samples, that is, a substituional Sn atom on a Se site[10(a)] that creates species Sn_{Se}^{2-}. This assumption is supported by the band structure calculation, which reveals that the Fermi level (Fr) is lowering to the valence band upon Sn occupation Se sites, as shown in Fig.3(d). In this case, in the stacking sequence Se–In–In–Se in the layered InSe structure, there exist interactive donor-acceptor defect pairs ($2Sn_{In}^{+}$ and Sn_{Se}^{2-}) (DADPs). The reaction between cations and anions in DADPs can lead to their partial annihilation, thus resulting in the reduction of the defect concentration and the number of species (Sn_{In}^{+} and Sn_{Se}^{2-}).[29] Since the neutralization between the cationic Sn^{+} and the neighbor anionic Sn^{2-} leads to the short range ordering tendency of the structure, therefore, the phonon scattering weakens and the lattice part κ_L increases drastically in the highly Sn-doped sample (x=0.02).

4. Conclusions

We have in this work prepared different Sn-doped InSe and observed an enhancement in carrier concentration (n) at $x \leq 0.01$ that is mainly caused by the creation of active donor defect Sn_{In}^{+} upon Sn's preferential occupation on the In site. However, this enhancement is limited because of the formation of an intermediate band in the middle of the bandgap, which acts as an annihilation center for electrons and holes. Besides, the defect Sn_{In}^{+} also act as scattering centers for phonons. Therefore, the lattice thermal conductivity (κ_L) reduces and the TE performance improves remarkably at a proper Sn content.

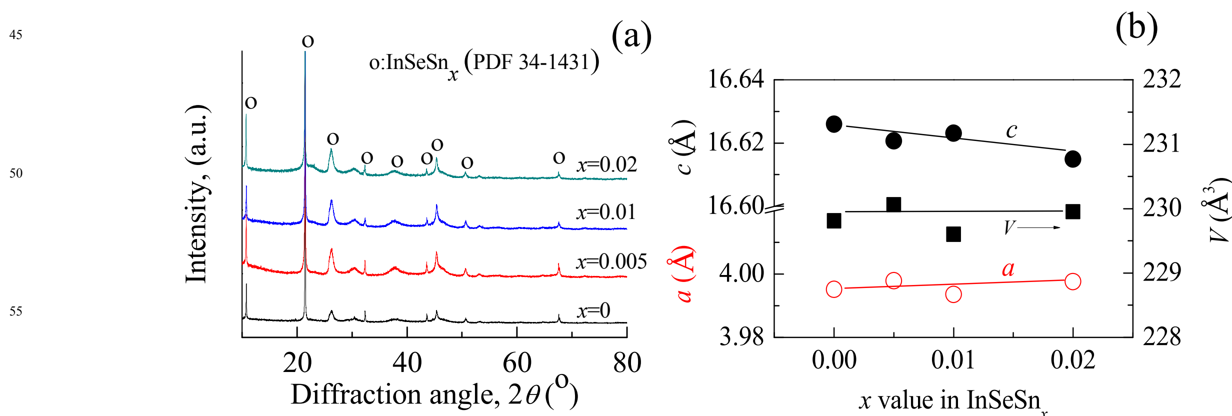

Fig.1 (a) The x-ray diffraction patterns of $InSeSn_x$ (x=0, 0.005, 0.01, 0.02) powders, (b) Lattice constants (a,c,V) as a function of x value.

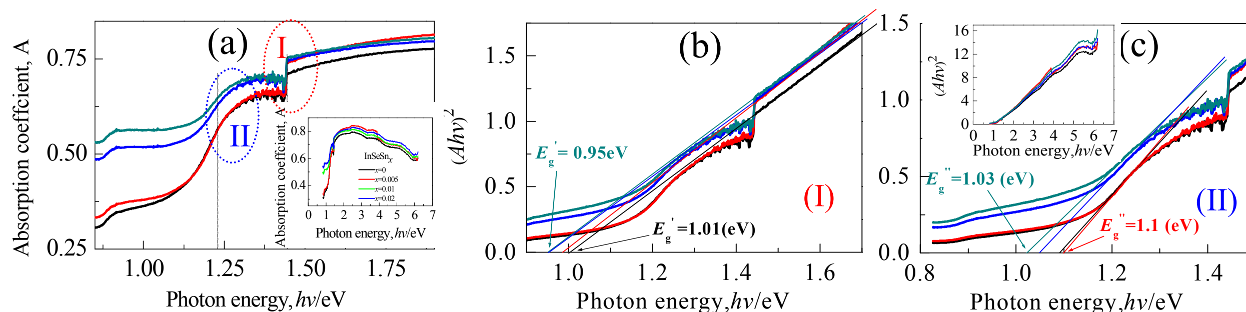

Fig.2 (a) Absorption coefficients (A) of different Sn contents (x) in InSe as a function of photon energy (hv), an insert is the full spectra $A(hv)$; (b) Experimentally determined bandgaps (E_g) from the first absorption edge (I) ; (c) Experimentally determined bandgaps (E_g) from the second absorption edge (II), an insert is the relations of $(Ahv)^2$ with photon energy (hv).

RSC Advances Accepted Manuscript

 This journal is © The Royal Society of Chemistry [year]

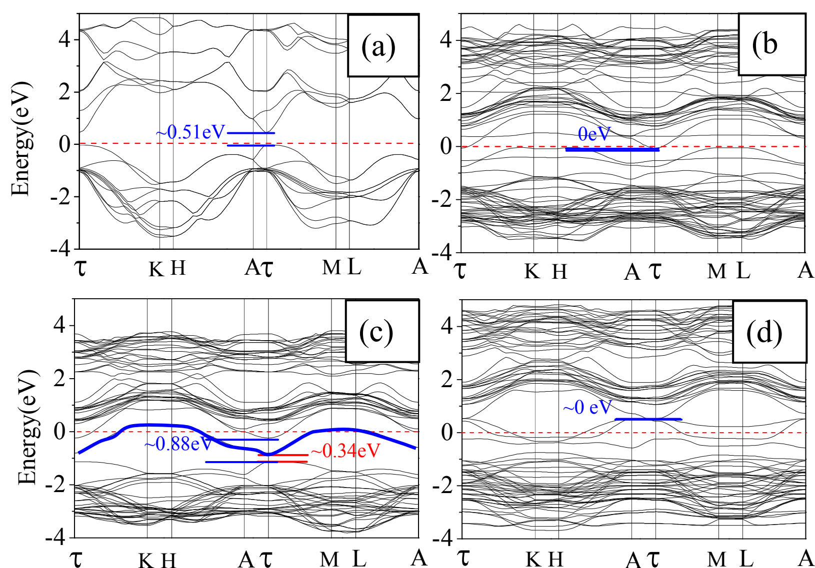

Fig.3 Calculated band structures InSeSn$_x$. (a) Virgin InSe with E_g= ~0.51eV; (b) An occupation of Sn in interstitial sites (In$_i$); (c) An occupation of Sn in In lattice sites with E_g= ~0.88eV, besides, there is an intermediate band in blue line; (d) An occupation of Sn in Se vacancies (V_{Se}) with E_g= ~0.40eV.

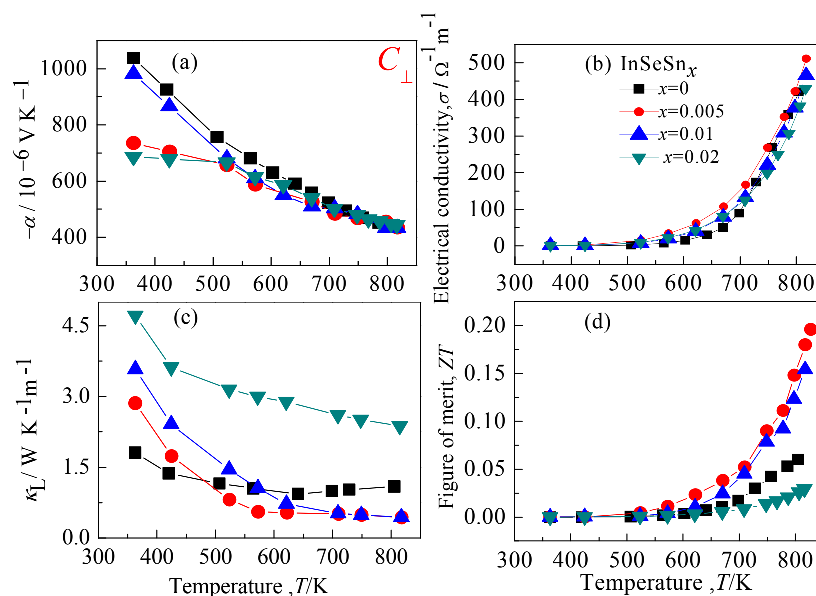

Fig. 4 Thermoelectric properties of InSeSn$_x$ (x=0, 0.005, 0.01, 0.02) samples perpendicular to the pressing direction ($C\perp$). (a) Seebeck coefficients (α), (b) Electrical conductivities (σ), (c) Lattice thermal conductivities (κ_L), an insert is a total κ, (d) Dimensionless figure of merit (ZT).

RSC Advances Accepted Manuscript

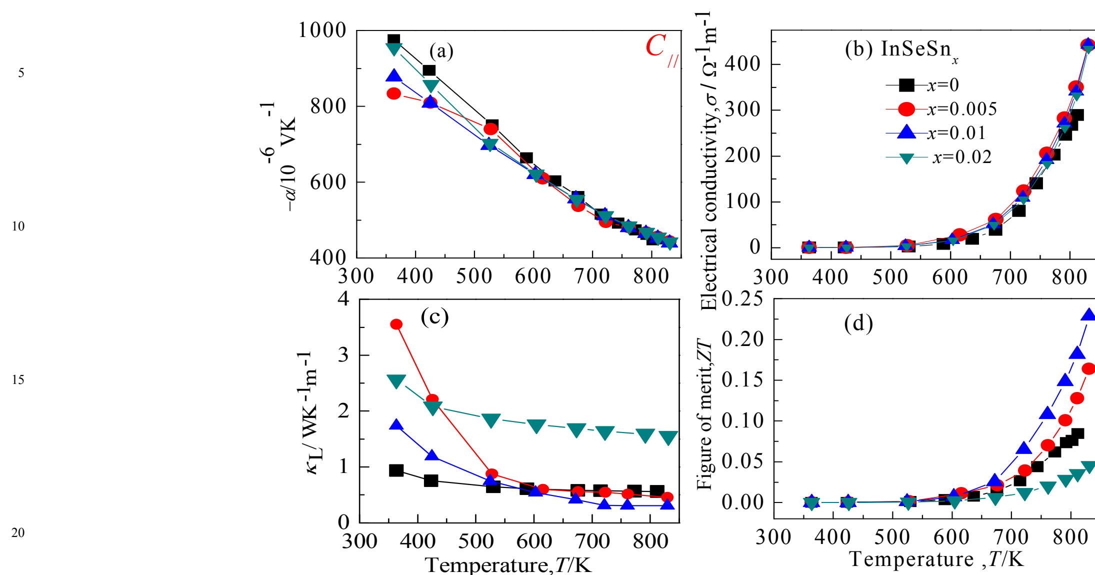

Fig. 5 Thermoelectric properties of $InSeSn_x$ (x=0, 0.005, 0.01, 0.02) samples along the pressing direction ($C_{//}$). (a) Seebeck coefficients (α), (b) Electrical conductivities (σ), (c) Lattice thermal conductivities (κ_L), (d) Dimensionless figure of merit (ZT).

Table 1 Carrier concentrations (n), mobility (μ) and effective mass (m^*) of different compounds $InSeSn_x$ at 360K.

Samples	x	R_H (m^3/C)	Carrier concentration, n [$1/m^3$]	Mobility, μ [$m^2V^{-1}s^{-1}$]	σ[$\Omega^{-1}m^{-1}$]	Remarks
$InSeSn_x$ ($C_\perp$)	0	-2.43×10^{-2}	2.57×10^{20}	1.68×10^{-3}	0.06	
	0.005	-6.84×10^{-3}	9.14×10^{20}	1.43×10^{-2}	2.09	
	0.01	-9.82×10^{-3}	6.36×10^{20}	1.06×10^{-2}	1.02	
$InSeSn_x$ ($C_{//}$)	0	-5.45×10^{-2}	1.15×10^{20}	3.06×10^{-3}	0.06	
	0.005	-8.64×10^{-3}	7.23×10^{20}	4.94×10^{-2}	5.71	
	0.01	-8.95×10^{-3}	6.98×10^{20}	1.38×10^{-3}	0.15	
Sn-doped InSe			0.70×10^{22}~5.70×10^{22} at RT	5.62×10^{-2}~11.0×10^{-2} at RT		*Ref.*10, 11

RSC Advances Accepted Manuscript

This journal is © The Royal Society of Chemistry [year]

Acknowledgements

This work is supported by the National Natural Science Foundation of China (51171084, 50871056), Zhejiang Provincial Natural Science Foundation (LY14E010003), and Natural Science Foundation of Ningbo (2014A610016).

5 ## Notes and references

[a] Materials Science and Engineering College, Taiyuan University of Technology, Taiyuan 030024, China
[b] School of Materials, Ningbo University of Technology, Ningbo 315016, China.

* Corresponding author, Jiaolin Cui, E-mail: cuijiaolin@163.com; sxchenshaoping@163.com

10

Electronic Supplementary Information (ESI) available: [Supporting Information is available from the RSC Online Library or from the author.]. See DOI: 10.1039/b000000x/

15

20

25

30

35

40

45

50

55

60

65

RSC Advances Accepted Manuscript

REFERENCES

1. J. P.Heremans, V. Jovovic, E. S. Toberer, A. Saramat, K. Kurosaki, A. Charoenphakdee, S.Yamanaka and G. J. Snyder, *Science*, 2008, **321**, 554.
2. (a) Y. Pei, X. Shi, A. LaLonde, H. Wang, L. Chen and G. J. Snyder, *Nature*, 2011, **473**, 66; (b) W. Liu, X. Tan, K. Yin, H. Liu, X. Tang, J. Shi, Q. Zhang and C. Uher, *Phys. Rev. Lett.*, 2012, **108**, 166601.
3. L.D.Hicks, and M. S.Dresselhaus, *Phys. Rev. B*, 1993, **47**, 12727.
4. J.P.Heremans, C. M.Thrush and D. T.Morelli, *Phys. Rev. B*, 2004, **70**, 115334.
5. K.F.Hsu, S.Loo, F.Guo, W.Chen, J.S.Dyck, C.Uher, T.Hogan, E.K.Polychroniadis and M.G. Kanatzidis, *Science*, 2004, **303**, 818.
6. K.Biswas, J. He, I. D. Blum, C.Wu, T.P.Hogan, D.N.Seidman, V.P.Dravid and M.G.Kanatzidis, *Nature*, 2012, **489**, 414.
7. (a)G. Han, Z.Chen, J. Drennan and J. Zou, *Small*, 2014, **10**, 2747; (b) H. G. Si, Y.X.Wang, Y.L.Yan and G. B. Zhang, *J. Phys. Chem. C*, 2012, **116**, 3956.
8. (a) J.Rhyee, K.H.Lee, S.M.Lee, E.Cho, S.II Kim, E.Lee, Y.S.Kwon, J.H.Shim and G.Kotliar, *Nature*, 2009, **459**, 965; (b) Y. Luo, J. Yang, G. Li, M. Liu, Y. Xiao, L. Fu, W. Li, P. Zhu, J. Peng, S. Gao and J. Zhang, *Adv. Energy Mater*., 2014, **4**, 1300599.
9. J. Cui, L. Wang, Z. Du, P. Ying and Y. Deng, *J. Mater. Chem. C*, 2015, **3**, 9069.
10. (a) B. Marí, A. Segura and A. Chevy, *Appl. Phys. A*, 1988, **46**, 125; (b) A. Chevy, *J. Appl. Phys*., 1984, **56**, 978.
11. A. Segura, K. Wünstel and A. Chevy, *Appl. Phys. A*, 1983, **31**,139.
12. (a) K. Imai, K. Suzuki, T. Hgag, Y. Hasegawa and Y. Abe, *J. Cryst. Growth*, 1981, **54**, 501; (b) C.Julian, E.Hatzikraniotis, A.Chevy and K.kambas, *Mater. Res. Bull.*, 1985, **20**, 287.
13. G. J. Snyder and E. S. Toberer, *Nat. Mater*., 2008,**7**, 105.
14. (a) V.V. Gridin, C. Kasl, J.D. Comins and R.Besermana, *J.Appl.Phys*.,1992,**71**,12, 6069; (b) S.Shigetomi, H.Ohkubo, T.Ikari and H.Nakashima, *J. Appl. Phys*., 1989, **66**, 3647.
15. T. Colakoğlu and M. Parlak, *Appl. Surf. Sci*., 2008, **254**, 1569.
16. (a) A.A.Yadav and S.D. Salunke, *J.Alloys Compds*., 2015, **640**, 534; (b) S. Johnsen, J.He, J. Androulakis, V. P. Dravid, I. Todorov, D.Y. Chung and M. G. Kanatzidis, *J. Am. Chem. Soc*., 2011, **133**,3460.
17. S. Popović, A. Tonejc, B. G. Plenković, B. Čelustka and R. Trojko, *J. Appl. Cryst*., 1979, **12**, 416.
18. (a) M. Balkanski, P. G. D. Costa and R. F. Wallis, *Phys. Stat. Sol*. (b), 1996, **194**, 175; (b) S. I. Drapak, V.B.Orletskiĭ, Z.D. Kovalyuk, V.V.Netyaga and V.D.Fotiĭ, *Tech. Phys. Lett.,* 2003, **29**, 480.
19. N. Kuroda, I. Munakata and Y. Nishina, *Solid State Commun*., 1980, **33**, 687.
20. K. Otte, G. Lippold, D. Hirsch, A. Schindler and F. Bigl, *Thin Solid Films*, 2000, **361-362**, 498.
21. H. Zhou and J. Park, *Phys. Sta. Sol. (a)*, 2015, **212**, 414.
22. I. Jendrzejewska, P.Zajdel, J.Heiman, J. Krok-Kowalski, T.Mydlarz and J. Mrzigod, *Mater. Res. Bull.*, 2012, **47**, 1881.
23. J. F. Moulder and J. Chastain, *Handbook of X-ray Photoelectron Spectroscopy: A Reference Book of Standard Spectra for Identification and Interpretation of XPS Data*, Perkin–Elmer Corporation, Physical Electronics Division, Eden Prairie, Minnesota, 1992, pp. 92.
24. (a) G. Pang, H. Jin, Y. Li , Q. Wan, Y. Sun, S. Feng and A. Gedanken, *J. Mater. Sci*., 2006, **41**, 1429; (b) M. Huang, Z. Hameiri, A. G. Aberle and T. Mueller, *Vacuum*, 2015, **121**, 187; (c) H. Lu, B. Lin, S. Chen and P. Shen, *J. Phys. Chem. C*, 2011, **115**, 24577; (d) Y. Hosogi, Y. Shimodaira, H. Kato, H. Kobayashi and A. Kudo, *Chem. Mater*., 2008, **20**, 1299; (e) D. Maestre, A. Cremades, L. Gregoratti and J. Piqueras, *J. Phys. Chem. C*, 2010, **114**, 3411.
25. (a) D. Errandonea, A. Segura, F. J. Manjón and A. Chevy, *Semicond. Sci. Technol*. 2003, **18**, 241; (b) D. J. Chadi and K.J.Chang, *Phys. Rev. B*, 1989, **39** 10063; (c) Y. Takeda, X. C. Gong, Y. Zhu and A. Sasaki, *Japan. J. Appl. Phys.* 1987, **26,** L273.
26. (a) Z.Lin , L.Chen , L.Wang , J. Zhao and L.Wu, *Adv. Mater*., 2013, **25**, 4800; (b) J. Rhyee, K. Ahn, K. H. Lee, H. S. Ji and J. Shim, *Adv. Mater*., 2011, **23**, 2191.

RSC Advances Accepted Manuscript

This journal is © The Royal Society of Chemistry [year]

27. Y. Zhai, Q. Zhang, J. Jiang, T. Zhang, Y. Xiao, S. Yang and G. Xu, *J. Alloys Compds*., 2013, **553**, 270.

28. (a) V. Leute and A. Zeppenfeld, *Ber. Bunsenges. Phys. Chem*. 1994, **98**, 233; (b) M. Bredol and V. Leute, *Ber. Bunsenges. Phys. Chem.* 1986, **90**, 714.

29. (a) S. B. Zhang, S. H. Wei and A. Zunger, *Phys. Rev. Lett*., 1997, **78**, 4059; (b) C. Rincón, S.M. Wasim and G. Marín, *Appl. Phys. Lett*., 2002, **80**, 998.

RSC Advances Accepted Manuscript

Table of contents:

Sn preferentially occupies In sites, which creates a defect Sn_{In}^{+} and intermediate band, thus tailoring the thermoelectric performance of InSe.

ToC figure:

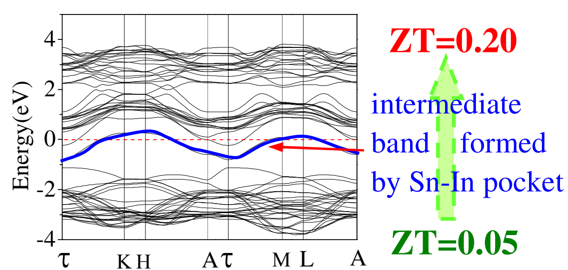

RSC Advances Accepted Manuscript